Research Square

Preprints are preliminary reports that have not undergone peer review.
They should not be considered conclusive, used to inform clinical practice,
or referenced by the media as validated information.

Seismic Pounding Mitigation of Adjacent Buildings through Nonlinear Stiffness Tuning: Impact-Onset Boundaries and Separation-Gap Design

Alvaro H. Salas

ahsalass@unal.edu.co

Universidad Nacional de Colombia

Vugar Abdullayev

Azerbaijan University of Architecture and Construction

Research Article

Keywords:

Posted Date: November 12th, 2026

DOI: https://doi.org/10.21203/rs.3.rs-11224819/v1

License: This work is licensed under a Creative Commons Attribution 4.0 International License.
Read Full License

Additional Declarations: No competing interests reported.

Seismic Pounding Mitigation of Adjacent Buildings through Nonlinear Stiffness Tuning: Impact-Onset Boundaries and Separation-Gap Design

Alvaro H. Salas[1,*] Vugar Abdullayev[2]

[1] Department of Mathematics and Statistics, FIZMAKO Research Group, Universidad Nacional de Colombia, Sede Manizales, Manizales, Colombia

[2] Azerbaijan University of Architecture and Construction, Baku, Azerbaijan

[*] Corresponding author: ahsalass@unal.edu.co; ORCID: 0000-0001-9343-6062

Abstract

Insufficient separation between adjacent buildings can produce repeated impact, large local contact forces and redistribution of seismic demand during strong ground motion. Conventional reduced-order pounding models usually assume linear structural response before contact and introduce nonlinearity only through the impact element. This study investigates a different mitigation mechanism in which the dominant lateral response of one building contains an effective cubic stiffness that can be tuned to modify the relative motion across the seismic joint. An exact pre-impact criterion is first established for arbitrary ground acceleration: the minimum separation required to prevent first contact is determined exclusively by the maximum oriented relative displacement of the uncoupled adjacent structures and is independent of the subsequent contact constitutive law. For harmonic excitation, the nonlinear structural response is reduced to a cubic amplitude equation whose discriminant identifies single- and multiple-response regimes and yields closed-form fold and cusp boundaries. These response branches are then mapped directly into branch-dependent seismic separation requirements through their relative amplitude and phase. For the representative building pair, at $\Omega/\omega_2 = 1.20$ and $a_0 = 0.12g$, one stable response state requires approximately 0.200 m of clearance, whereas a coexisting nonlinear state requires only about 0.034 m because the structures move nearly in phase. Treating the cubic stiffness as a design parameter produces a root-robust safe region and an optimum near 2.44×10^9 N/m^3, for which the predicted onset gap is reduced to approximately 26.7 mm. Nonlinear Hertz-type impact simulations confirm the transition between repeated pounding and impact-free response, while broadband excitation verifies the general first-impact criterion. The results demonstrate that appropriately tuned structural nonlinearity can act as a passive pounding-mitigation mechanism by simultaneously controlling response amplitude and phase. The proposed onset boundaries and separation-gap maps provide a computationally inexpensive screening framework for the preliminary design and assessment of adjacent structures before detailed nonlinear contact analysis.

Keywords: adjacent buildings; seismic pounding; separation gap; nonlinear stiffness; passive mitigation; structural dynamics; impact onset; earthquake engineering; design maps.

1 Introduction

Seismic pounding between adjacent buildings remains a practical concern in dense urban environments because the available joint width is often constrained by property lines, architectural requirements and existing construction. When neighboring structures respond out of phase, closure of the separation gap can generate local crushing, large acceleration pulses, shear amplification and redistribution of structural demand [1, 4, 6, 9]. Current assessment procedures therefore require a reliable estimate of the relative displacement demand before detailed contact-force calculations are undertaken.

Most reduced pounding models assume that both neighboring structures remain linear before impact and place the principal nonlinearity in the contact element. That approach is appropriate for many applications, but it cannot represent structural components whose effective lateral stiffness varies with amplitude. Braces, elastic restraints, isolation devices, geometric effects and reduced smooth restoring curves can introduce amplitude-dependent stiffness before contact. In such cases, the seismic-joint demand depends not only on the individual peak responses but also on nonlinear detuning, branch transitions and the phase relation between the two structures.

This study considers the simplest asymmetric configuration that retains those mechanisms: Building 1 is represented by a linear dominant mode and Building 2 by a Duffing-type dominant mode. The objective is not to replace detailed nonlinear building models, but to obtain transparent design relations that identify when structural nonlinearity increases or decreases the separation required to avoid impact. A stabilized gravity-loaded sway mechanism is used only to illustrate one physical route to a cubic stiffness; in project-specific applications the cubic coefficient is an effective generalized parameter obtained from model reduction, nonlinear static analysis, identification or a device restoring law.

A key distinction is made between *impact onset* and *post-contact severity*. Before first contact, the contact force is exactly zero. The critical gap is therefore governed entirely by the uncoupled pre-impact trajectories, whereas the chosen Hertz, viscoelastic or restitution model affects the response only after the gap closes. This observation leads to an exact onset criterion for arbitrary common ground acceleration and provides a consistency check for nonlinear impact simulations.

The paper develops four linked engineering contributions. First, an exact seismic-joint onset criterion is obtained for arbitrary excitation. Second, the nonlinear response boundaries are characterized analytically so that single- and multiple-response regimes can be identified before time integration. Third, each admissible nonlinear state is mapped into a branch-specific separation demand, producing design-oriented safe-gap maps. Fourth, the effective cubic stiffness is treated as a passive mitigation variable, leading to an explicit safe region and an analytically identifiable optimum for a representative harmonic design point. Nonlinear Hertz-type simulations and broadband

excitation are used to verify the predicted transition between repeated pounding and impact-free response.

The idealized configuration and unilateral gap convention are illustrated in Figure 1. The central structural insight is that pounding risk is controlled by relative-response geometry. A larger displacement amplitude of the nonlinear building need not imply a larger joint demand if nonlinear detuning simultaneously moves the two structures toward a favorable phase relation. This mechanism motivates the nonlinear-stiffness tuning framework developed below.

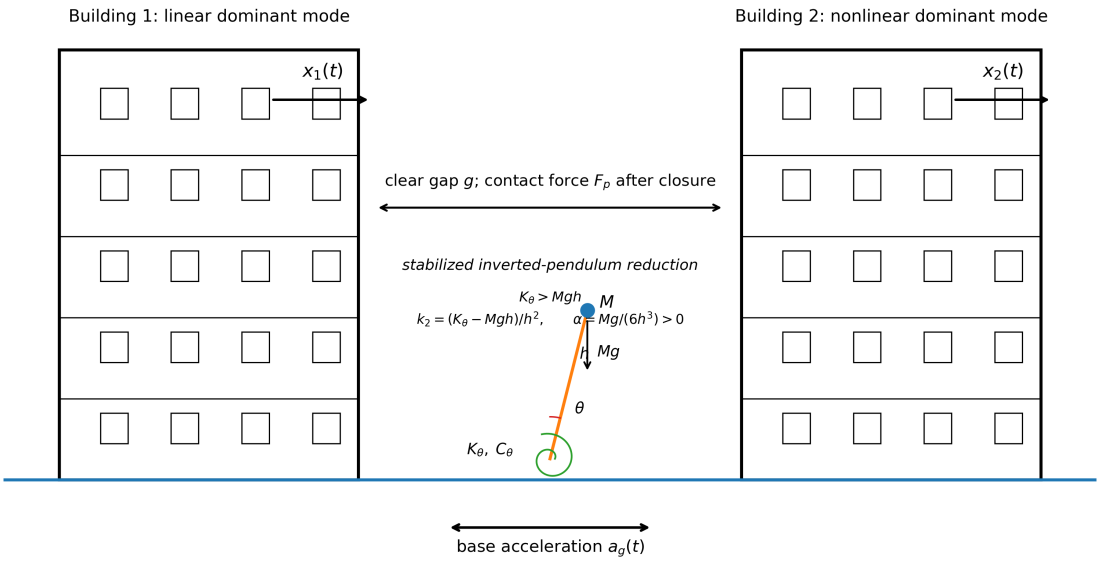


Figure 1: Physical interpretation of the asymmetric adjacent-building model. Building 1 is represented by a linear dominant mode. Building 2 has an effective nonlinear mode; the central inset shows a stabilized inverted-pendulum mechanism that generates a positive cubic stiffness after small-angle reduction. Contact is inactive until the relative displacement closes the clear gap g.

2 Adjacent-building model and seismic-joint mechanics

2.1 Equations of motion

Let $x_1(t)$ and $x_2(t)$ denote the horizontal displacements relative to the ground. Building 1 is linear, whereas Building 2 contains a cubic restoring term. The coupled equations are

$$m_1\ddot{x}_1 + c_1\dot{x}_1 + k_1x_1 = -m_1a_g(t) - F_p, \tag{1}$$

$$m_2\ddot{x}_2 + c_2\dot{x}_2 + k_2x_2 + \alpha x_2^3 = -m_2a_g(t) + F_p. \tag{2}$$

The sign convention assumes Building 1 lies to the left of Building 2. Define

$$\delta(t) = x_1(t) - x_2(t) - g, \tag{3}$$

where $g > 0$ is the initial clear gap. Contact is possible only when $\delta > 0$.

For post-contact simulations we use the regularized Hertz-type law

$$F_p = \begin{cases} 0, & \delta \le 0, \\ \max\left\{k_H \delta^{3/2} + c_H \delta^{1/2}\dot{\delta}, 0\right\}, & \delta > 0, \end{cases} \tag{4}$$

which prevents tensile contact. The precise law is not needed for the onset theorem below; it is used only to quantify post-contact response. Nonlinear impact models of this form and their calibration issues are discussed in detail in the impact-model literature [8, 10].

The linear natural frequencies and damping ratios are

$$\omega_i = \sqrt{k_i/m_i}, \qquad \zeta_i = \frac{c_i}{2m_i\omega_i}. \tag{5}$$

For $\alpha > 0$, Building 2 is hardening; for $\alpha < 0$, it is softening.

2.2 A stabilized inverted-pendulum route to the Duffing term

A simple mechanical derivation clarifies why a cubic restoring term is structurally plausible. Consider a generalized sway mechanism represented by a point mass M at height h, a base rotational spring K_θ, rotational damping C_θ, and a small rotation $\theta(t)$ measured from the vertical unstable orientation. Under horizontal base acceleration, the exact rotational equation is

$$Mh^2\ddot{\theta} + C_\theta\dot{\theta} + K_\theta\theta - Mgh\sin\theta = -Mh\,a_g(t)\cos\theta. \tag{6}$$

Stability of the vertical equilibrium requires $K_\theta > Mgh$. Using $\sin\theta = \theta - \theta^3/6 + O(\theta^5)$ and $\cos\theta = 1 + O(\theta^2)$, and introducing the lateral coordinate $x = h\theta$, gives

$$M\ddot{x} + \frac{C_\theta}{h^2}\dot{x} + \frac{K_\theta - Mgh}{h^2}x + \frac{Mg}{6h^3}x^3 = -Ma_g(t) + O\left(\frac{x^5}{h^5}, \frac{a_g x^2}{h^2}\right). \tag{7}$$

Hence the reduced coefficients are

$$c_{\text{eff}} = \frac{C_\theta}{h^2}, \qquad k_{\text{eff}} = \frac{K_\theta - Mgh}{h^2}, \qquad \alpha_{\text{geom}} = \frac{Mg}{6h^3} > 0. \tag{8}$$

Proposition 1 (Geometric Duffing reduction)**.** *A gravity-loaded sway mechanism stabilized by a sufficiently stiff rotational restraint has, to cubic order, a hardening Duffing restoring force. More general modal models may have either sign of α because braces, connections, isolators, distributed geometric effects or local constitutive softening can alter the effective cubic coefficient.*

The derivation is used here as a physical interpretation, not as a literal claim that a multi-storey building behaves as a rigid pendulum. In a frame model, m_2, k_2, c_2 and α are generalized modal quantities obtained by projection, identification or model reduction. This distinction is important when transferring the analytical results to project-specific structures.

2.3 Exact first-impact threshold under arbitrary excitation

Let $(x_1^{(0)}, x_2^{(0)})$ denote the solution of the *uncoupled* pre-impact problem obtained by setting $F_p = 0$ in Eqs. (1)–(2). Define

$$D_0(t) = x_1^{(0)}(t) - x_2^{(0)}(t). \tag{9}$$

Theorem 1 (Exact onset criterion)**.** *For any unilateral contact law satisfying $F_p = 0$ whenever $\delta \le 0$, the critical gap over an observation interval $[0, T]$ is*

$$g_{\mathrm{cr}} = \max_{0 \le t \le T} D_0(t). \tag{10}$$

If $g > g_{\mathrm{cr}}$, contact cannot occur on $[0, T]$. If $g < g_{\mathrm{cr}}$ and D_0 is continuous, a first-contact time exists. Equality gives the limiting first-touch condition.

Proof. Before the first contact, $F_p = 0$, so the trajectories of the contact system and the uncoupled system are identical. Contact occurs when $D_0(t) - g = 0$ is reached from below. The three statements follow directly from the maximum of the continuous function D_0. □

The result is simple but useful. It remains exact even though Building 2 is nonlinear. The post-contact parameters k_H and c_H cannot affect the first-impact threshold, although they strongly affect peak force, overlap and rebound after contact. This provides a numerical consistency test: simulations with $g > g_{\mathrm{cr}}$ must remain contact-free regardless of the impact parameters.

3 Nonlinear response boundaries under harmonic excitation

3.1 First-harmonic equations

To expose the nonlinear resonance mechanism analytically, consider

$$a_g(t) = a_0 \cos \Omega t. \tag{11}$$

The common minus sign in the inertial forcing may be absorbed into a common phase shift and therefore does not affect the relative phase. The linear steady-state response has amplitude and phase

$$A_1 = \frac{m_1 a_0}{\sqrt{\Delta_1^2 + d_1^2}}, \qquad \phi_1 = \operatorname{atan2}(d_1, \Delta_1), \tag{12}$$

where

$$\Delta_i = k_i - m_i \Omega^2, \qquad d_i = c_i \Omega. \tag{13}$$

For Building 2, let $x_2 \approx A_2 \cos(\Omega t - \phi_2)$. Retaining the fundamental component $x_2^3 \approx (3/4)A_2^3 \cos(\Omega t - \phi_2)$ gives

$$A_2^2 \left[\left(\Delta_2 + q A_2^2 \right)^2 + d_2^2 \right] = F_2^2, \qquad q = \frac{3\alpha}{4}, \quad F_2 = m_2 a_0, \tag{14}$$

and

$$\phi_2 = \operatorname{atan2}\left(d_2, \Delta_2 + q A_2^2 \right). \tag{15}$$

Introducing $y = A_2^2$, Eq. (14) becomes the cubic polynomial

$$P(y) = q^2 y^3 + 2\Delta_2 q y^2 + (\Delta_2^2 + d_2^2) y - F_2^2 = 0. \tag{16}$$

Thus the number of candidate harmonic amplitudes can be determined algebraically.

3.2 Polynomial discriminant and response multiplicity

For a cubic $ay^3 + by^2 + cy + d$, the polynomial discriminant distinguishes one and three distinct real roots. Applied to Eq. (16), direct simplification gives

$$\mathcal{D}_y = -q^2 \left[4 d_2^2 (\Delta_2^2 + d_2^2)^2 + 4\Delta_2 F_2^2 q (\Delta_2^2 + 9 d_2^2) + 27 F_2^4 q^2 \right]. \tag{17}$$

When $\mathcal{D}_y > 0$, three distinct real roots exist; when $\mathcal{D}_y < 0$, there is one real root; and $\mathcal{D}_y = 0$ marks a repeated root. Physical harmonic states additionally require $y > 0$. Figure 2 shows the positive roots for the baseline hardening case.

The three-root region can also be displayed directly in the frequency–forcing plane. Figure 3 plots the number of positive roots obtained from Eq. (16); the wedge opens from the analytic cusp derived next.

3.3 Closed fold and cusp formulas

The folds of the amplitude relation satisfy $P(y) = 0$ and $P'(y) = 0$. Since

$$P'(y) = 3q^2 y^2 + 4\Delta_2 q y + (\Delta_2^2 + d_2^2), \tag{18}$$

the fold amplitudes are

$$y_\pm = \frac{-2\Delta_2 \pm \sqrt{\Delta_2^2 - 3 d_2^2}}{3q}. \tag{19}$$

A necessary condition for folds is

$$\Delta_2^2 \geq 3 d_2^2, \tag{20}$$

plus $y_\pm > 0$.

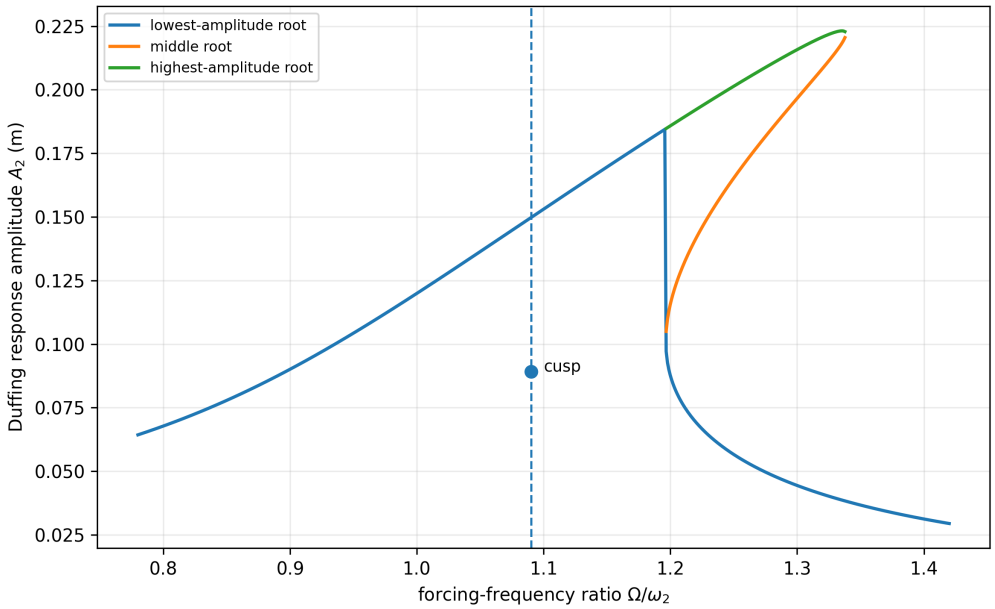


Figure 2: Positive first-harmonic Duffing amplitudes for the baseline hardening building at $a_0 = 0.12g$. The analytic cusp is marked. The middle root in the three-root region is the familiar transition branch; time integration confirms coexistence of lower and upper attracting responses at selected frequencies.

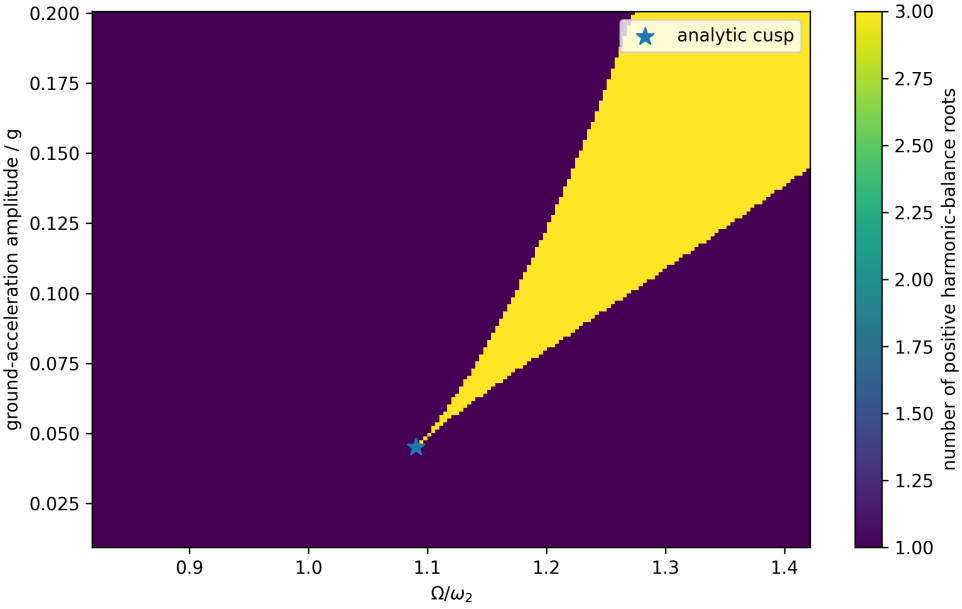


Figure 3: Number of positive harmonic-balance roots as a function of forcing-frequency ratio and ground-acceleration amplitude. The star is the closed-form cusp predicted by Eqs. (22)–(23).

At the cusp, $P = P' = P'' = 0$. Because $P'' = 6q^2y + 4\Delta_2 q$, one obtains

$$y_c = -\frac{2\Delta_c}{3q}, \qquad \Delta_c = -\operatorname{sgn}(q)\sqrt{3}\, d_c. \tag{21}$$

Using $\Delta_c = k_2 - m_2\Omega_c^2$ and $d_c = c_2\Omega_c$, the cusp frequency is

$$\Omega_c = \begin{cases} \dfrac{\sqrt{3}c_2 + \sqrt{3c_2^2 + 4m_2k_2}}{2m_2}, & q > 0, \\ \dfrac{-\sqrt{3}c_2 + \sqrt{3c_2^2 + 4m_2k_2}}{2m_2}, & q < 0. \end{cases} \tag{22}$$

Finally,

$$F_c^2 = \frac{8d_c^3}{3\sqrt{3}\,|q|}, \qquad a_{0,c} = \frac{F_c}{m_2}, \qquad A_{2,c} = \sqrt{\frac{2d_c}{\sqrt{3}\,|q|}}. \tag{23}$$

Proposition 2 (Cusp threshold)**.** *For the first-harmonic Duffing model with $q \neq 0$, response multiplicity is born at the cusp defined by Eqs.* (22)–(23)*. For the baseline parameters of Table 1 with $\alpha = 2.0 \times 10^9$ N/m^3, the cusp occurs at*

$$\Omega_c/\omega_2 = 1.09035, \qquad a_{0,c} = 0.04518g, \qquad A_{2,c} = 0.08918 \text{ m}.$$

This closed threshold is useful because it predicts, before any time integration, the intensity level above which branch multiplicity can enter the pounding problem.

4 Branch-dependent seismic separation demand

4.1 Branch-specific harmonic onset criterion

For a given harmonic root $A_{2,j}$, the relative displacement is the difference of two sinusoids. Its amplitude is

$$A_{r,j} = \sqrt{A_1^2 + A_{2,j}^2 - 2A_1A_{2,j}\cos(\phi_1 - \phi_{2,j})}. \tag{24}$$

Therefore the harmonic first-impact threshold for branch j is

$$\boxed{g_{\mathrm{cr},j}^{\mathrm{HB}} = A_{r,j}}. \tag{25}$$

Corollary 1 (Branch-robust safe gap)**.** *If several dynamically admissible pre-impact harmonic states are possible at the same Ω and a_0, a conservative branch-robust harmonic separation is*

$$g_{\mathrm{safe}}^{\mathrm{HB}} = \max_j g_{\mathrm{cr},j}^{\mathrm{HB}}. \tag{26}$$

Figure 4 is the central analytical design result. In the multivalued frequency range, the clearance demand is itself multivalued. It does not follow the Duffing amplitude monotonically because the phase difference in Eq. (24) is equally important.

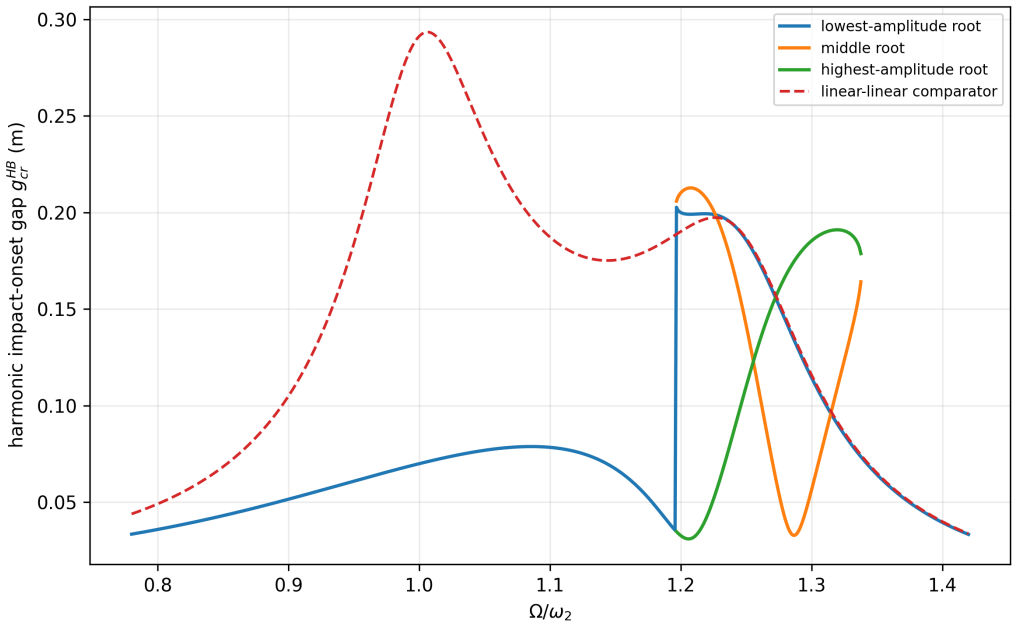


Figure 4: Branch-specific harmonic impact-onset gap for the linear–Duffing pair at $0.12g$, together with the linear–linear comparator. The nonlinear jump region changes both amplitude and phase, so the largest Duffing amplitude need not correspond to the largest separation demand.

This observation differs qualitatively from a peak-displacement-only interpretation. At $\Omega/\omega_2 = 1.20$, first-harmonic balance gives three positive roots. The lower and upper responses are both observed as attracting states in direct time integration for different initial conditions. The lower state has $A_2 \approx 0.088$ m but the buildings are strongly out of phase, producing $g_{\mathrm{cr}} \approx 0.200$ m. The upper state has $A_2 \approx 0.188$ m but the phase difference becomes small, reducing the relative-displacement maximum to approximately 0.034 m. Thus a nonlinear resonance jump can *reduce* pounding risk even while the nonlinear building vibrates with larger amplitude.

4.2 Why the phase reversal matters

For adjacent structures, individual amplitudes are not sufficient. Equation (24) shows two limiting cases. If the buildings are in phase,

$$A_r \approx |A_1 - A_2|, \tag{27}$$

whereas near opposition of phase,

$$A_r \approx A_1 + A_2. \tag{28}$$

A Duffing jump changes A_2 and ϕ_2 simultaneously. Consequently, the transition from a low branch to a high branch can either increase or decrease A_r. This is the mechanism behind the sharp valleys and branch exchanges visible in Figure 4.

The result also clarifies why separation rules based on independent peak displacements are necessarily conservative in some regimes and may fail to describe history-dependent nonlinear branch

selection in others. Code-based separation requirements remain essential for design compliance [17, 18]; the present criterion is intended as an analysis and screening tool rather than a replacement for mandatory provisions.

5 Verification with nonlinear impact simulations

5.1 Parameters and integration protocol

Table 1 lists the representative reduced-order parameters. The masses and periods are chosen to represent two neighboring medium-rise lateral modes with different elastic periods. The cubic coefficient is selected to produce a moderate hardening shift over displacement amplitudes of order 0.1–0.2 m. The contact constants are illustrative and are used only after first contact.

Table 1: Baseline parameters used in the reproducible calculations.

Parameter	Building 1 (linear)	Building 2 (Duffing)
Mass m	2.0×10^6 kg	2.4×10^6 kg
Small-amplitude period T	0.80 s	1.00 s
Damping ratio ζ	0.05	0.05
Linear stiffness k	1.2337×10^8 N/m	9.4748×10^7 N/m
Viscous damping c	1.5708×10^6 N s/m	1.5080×10^6 N s/m
Cubic coefficient α	0	2.0×10^9 N/m^3
Contact stiffness k_H	5.0×10^9 N/m$^{3/2}$	
Contact damping c_H	2.0×10^7 N s/m$^{3/2}$	

The equations are integrated with an adaptive eighth-order explicit Runge–Kutta method and tight relative/absolute tolerances. The maximum time step is reduced during impact simulations to resolve the short contact pulses. All plotted values can be regenerated by the supplied Python script.

5.2 Same earthquake amplitude, same gap, different branch: impact versus no impact

To isolate the effect of nonlinear branch selection, consider $a_0 = 0.12g$, $\Omega/\omega_2 = 1.20$ and $g = 0.10$ m. The uncoupled equations are first integrated for 96 forcing cycles so that the system settles onto a pre-impact attractor. Two initial conditions for Building 2 lead to two coexisting states. The state is then continued with the physical contact law switched on through the actual gap.

Figure 5 compares the oriented relative displacement. In the lower Duffing-amplitude basin, the pre-impact threshold is $g_{\mathrm{cr}} = 0.1998$ m, so the 0.10 m gap is insufficient and impacts occur. In the higher Duffing-amplitude basin, $g_{\mathrm{cr}} = 0.0342$ m and the same 0.10 m gap remains safely open. This is a branch-history effect: the forcing frequency, forcing amplitude, structural parameters and physical clearance are identical.

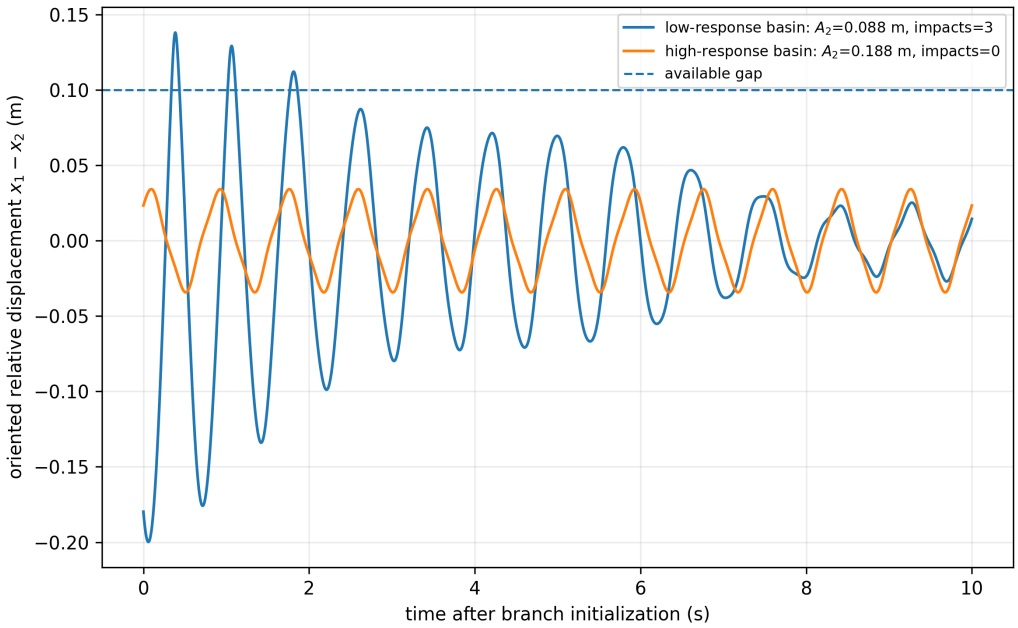


Figure 5: Direct integration at $\Omega/\omega_2 = 1.20$, $a_0 = 0.12g$ and $g = 0.10$ m. The lower Duffing-amplitude attractor produces gap closure and three impacts; the higher-amplitude attractor remains impact-free because the two structures move nearly in phase.

The corresponding contact-force history for the pounding branch is shown in Figure 6. Three impact episodes occur during the observation window, with a peak force of approximately 37.4 MN for the selected contact parameters. The peak force is not universal because it depends on k_H and c_H; the onset boundary is universal within the adopted pre-impact structural model.

5.3 Gap sweep and grazing behavior

Figure 7 varies the physical gap while keeping the pre-impact basin and excitation fixed. Peak force decreases as the gap approaches the onset threshold, but the impact count is not monotone. Near grazing, small repeated contacts can occur over multiple cycles before contact disappears completely. This is typical of vibro-impact systems and cautions against using impact count alone as a severity metric.

6 Separation-gap design maps for preliminary assessment

The analytical formulas can be evaluated cheaply over frequency and intensity. Figure 8 reports the branch-robust threshold from Eq. (26). The cusp marks the birth of response multiplicity. Above it, the required clearance can change sharply with excitation frequency because different nonlinear branches carry different phase relationships with the linear neighbor.

For design screening, the map can be read in three steps: (1) identify the dominant excitation frequency range relative to the nonlinear building's small-amplitude frequency; (2) estimate the

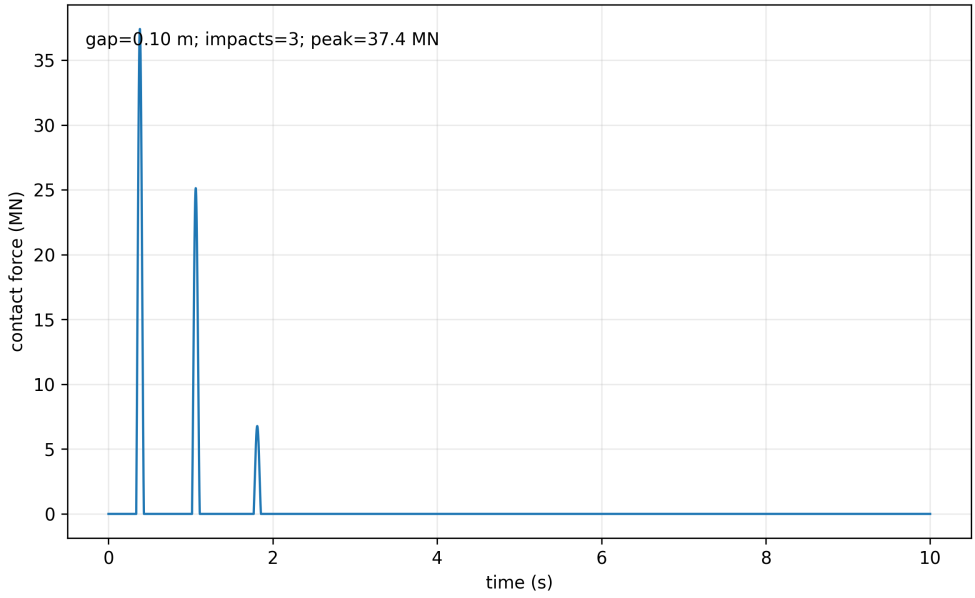


Figure 6: Hertz-type contact force for the pounding branch in Figure 5. The first-impact condition is fixed by the pre-contact relative displacement, whereas force severity depends on the impact constitutive parameters.

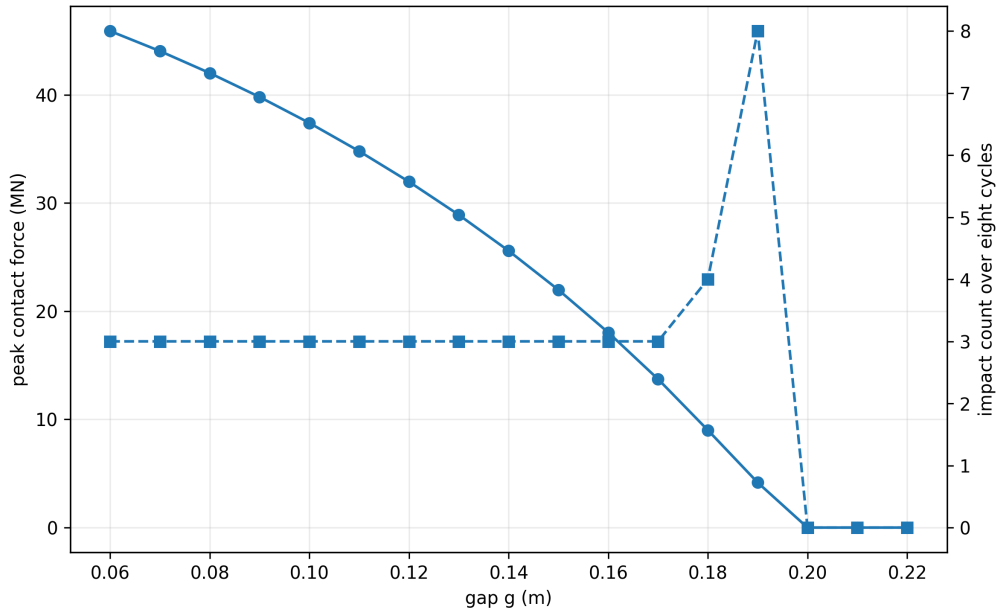


Figure 7: Peak contact force and number of impact episodes versus separation gap for the lower-amplitude pre-impact basin. Force vanishes once the gap exceeds the pre-impact threshold; the impact count can increase near grazing because weak contacts recur over successive cycles.

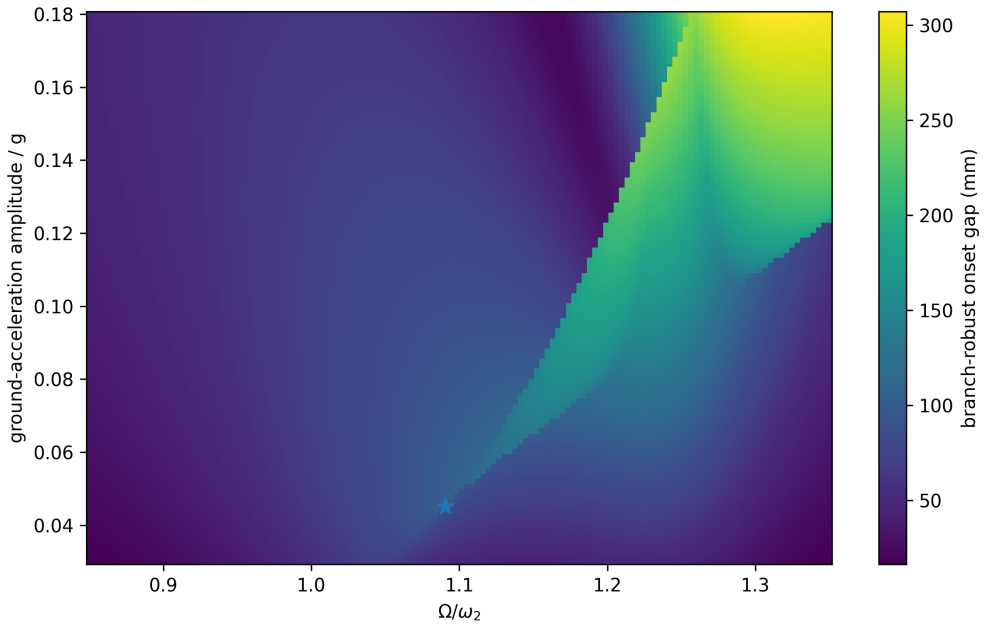


Figure 8: Branch-robust harmonic separation demand for the baseline hardening pair. The map takes the maximum branch-specific onset gap at each frequency and forcing amplitude.

effective forcing intensity for the reduced mode; and (3) compare the available joint width with the branch-robust threshold. If the available gap lies well above the map value, detailed impact analysis may be unnecessary for that reduced-order scenario. If it lies below, post-contact analysis is warranted.

The branch-robust construction is intentionally conservative when several harmonic states coexist. A less conservative analysis can use continuation from a known pre-earthquake state, but then branch selection and transient evolution must be modeled explicitly.

7 Broadband earthquake-type excitation and exact onset

The first-impact theorem is not restricted to harmonic forcing. To verify this point, a deterministic broadband pulse is constructed from three sinusoidal components under a smooth transient envelope and scaled to a PGA of $0.30g$. The excitation is not intended to represent a particular recorded earthquake; its purpose is to test the exact onset criterion under a nonstationary broadband input without invoking steady-state harmonic assumptions.

Figure 9 compares the uncoupled relative displacement for the linear–Duffing pair and for a linear–linear comparator with the same small-amplitude properties. The nonlinear system gives

$$g_{\mathrm{cr}}^{\mathrm{pulse}} = 0.0911 \text{ m}, \tag{29}$$

whereas suppressing the cubic term yields 0.2938 m. Thus the hardening response substantially

changes the relative-motion demand for this pulse. Contact simulations at $0.95g_{\mathrm{cr}}^{\mathrm{pulse}}$ and $1.05g_{\mathrm{cr}}^{\mathrm{pulse}}$ produce two impacts and zero impacts, respectively, confirming Theorem 1 to numerical tolerance.

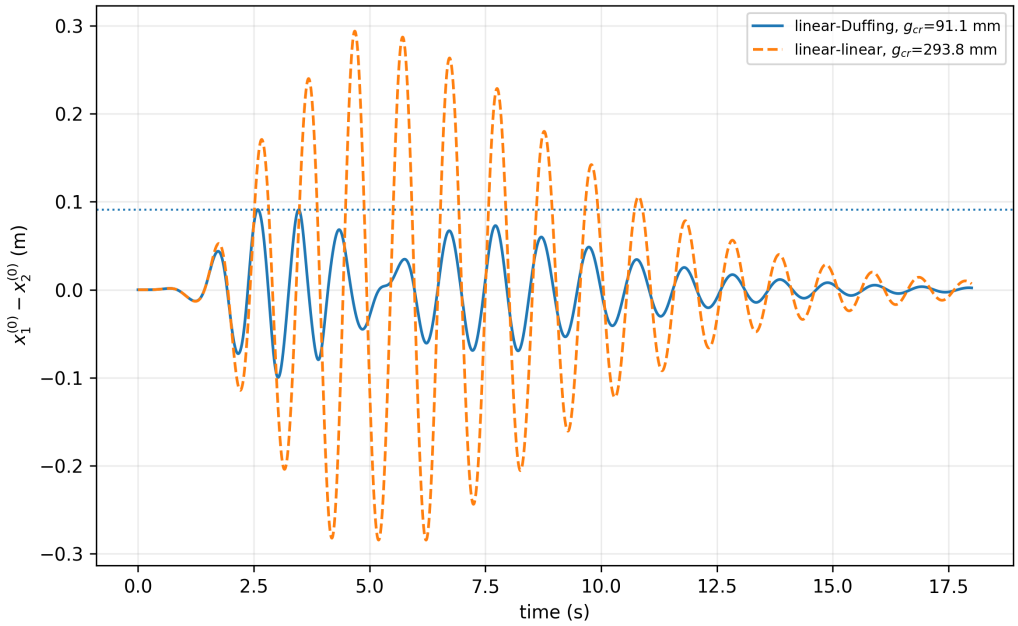


Figure 9: Pre-impact relative displacement under a broadband transient pulse (PGA $= 0.30g$). The exact nonlinear onset threshold is the maximum of the linear–Duffing relative displacement. The linear–linear comparator is shown to emphasize the effect of structural nonlinearity.

This example also separates two roles of the analytical development. For arbitrary records, Eq. (10) is exact but normally evaluated by integrating the uncoupled equations. For harmonic or narrow-band forcing, Eqs. (16)–(25) provide a nearly closed-form route that exposes multiplicity, folds, cusp thresholds and phase-driven changes in separation demand.

8 Effect of nonlinear stiffness on separation demand

The cubic coefficient controls the direction and strength of the nonlinear frequency shift. Figure 10 plots the branch-robust onset gap for several values of α at $a_0 = 0.12g$. Hardening ($\alpha > 0$) shifts the multivalued region to higher frequencies, while softening ($\alpha < 0$) shifts it to lower frequencies. The largest clearance demand can move by a substantial fraction of the linear resonance bandwidth even though the small-amplitude period is unchanged.

A useful dimensionless measure of cubic importance at a reference displacement X_r is

$$\eta = \frac{\alpha X_r^2}{k_2}. \tag{30}$$

For $X_r = 0.10$ m and the baseline parameters, $\eta \approx 0.211$. Thus the selected example represents a noticeable but not overwhelmingly dominant cubic correction over the response range of interest.

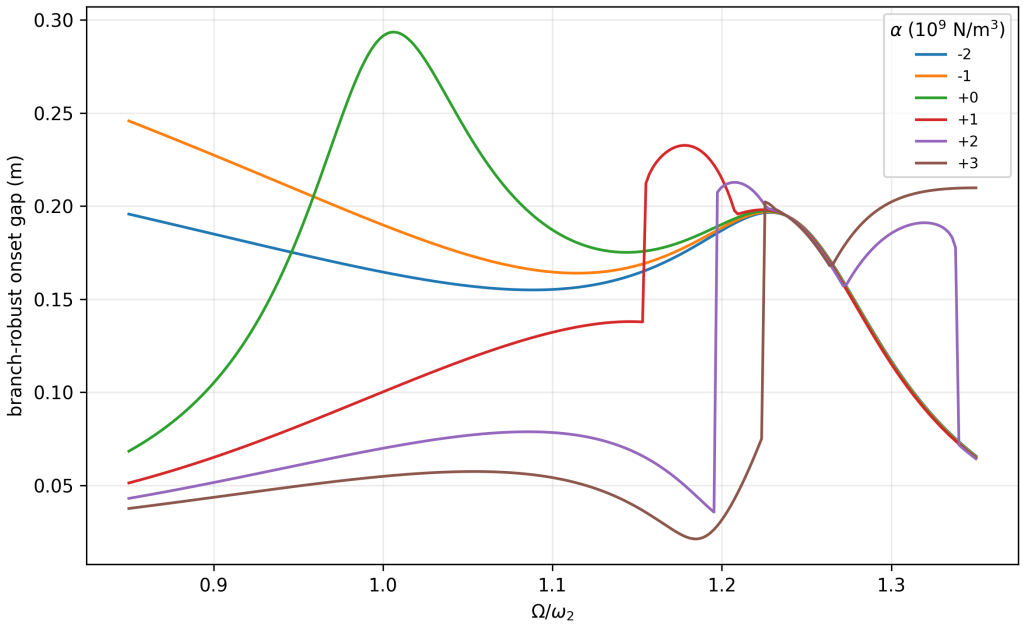


Figure 10: Sensitivity of branch-robust harmonic separation demand to the cubic coefficient. Positive α produces hardening and shifts the nonlinear features to the high-frequency side; negative α produces softening and shifts them to the low-frequency side.

9 Recovery of the conventional linear-building limit

The nonlinear model must recover the classical linear–linear pounding problem when $\alpha \to 0$. Let

$$Q = \Delta_2^2 + d_2^2, \qquad A_L = \frac{F_2}{\sqrt{Q}}. \tag{31}$$

For fixed finite F_2, expansion of Eq. (14) gives

$$A_2 = A_L - \alpha \frac{3\Delta_2 A_L^3}{4Q} + O(\alpha^2), \tag{32}$$

and the phase satisfies

$$\phi_2 = \phi_L - \alpha \frac{3 d_2 A_L^2}{4Q} + O(\alpha^2), \qquad \phi_L = \operatorname{atan2}(d_2, \Delta_2). \tag{33}$$

Thus the branch that remains at finite amplitude converges continuously to the ordinary linear frequency response. In particular,

$$\lim_{\alpha \to 0} g_{\mathrm{cr}}(\alpha) = g_{\mathrm{cr}}^{\mathrm{linear-linear}}. \tag{34}$$

The discriminant also explains why nonlinear multiplicity disappears. For small α with nonzero

damping,

$$\mathcal{D}_y = -\frac{9}{4}\alpha^2 d_2^2(\Delta_2^2 + d_2^2)^2 + O(\alpha^3) < 0, \tag{35}$$

so only one real harmonic-amplitude branch remains sufficiently close to the linear limit. At the cusp, Eqs. (21)–(23) imply

$$A_{2,c} = O(|\alpha|^{-1/2}), \qquad F_c = O(|\alpha|^{-1/2}). \tag{36}$$

Therefore the fold/cusp structure does not vanish discontinuously as $\alpha \to 0$; it is pushed to unbounded amplitude and forcing. Figure 11 illustrates this "cusp escape" for the baseline linear properties.

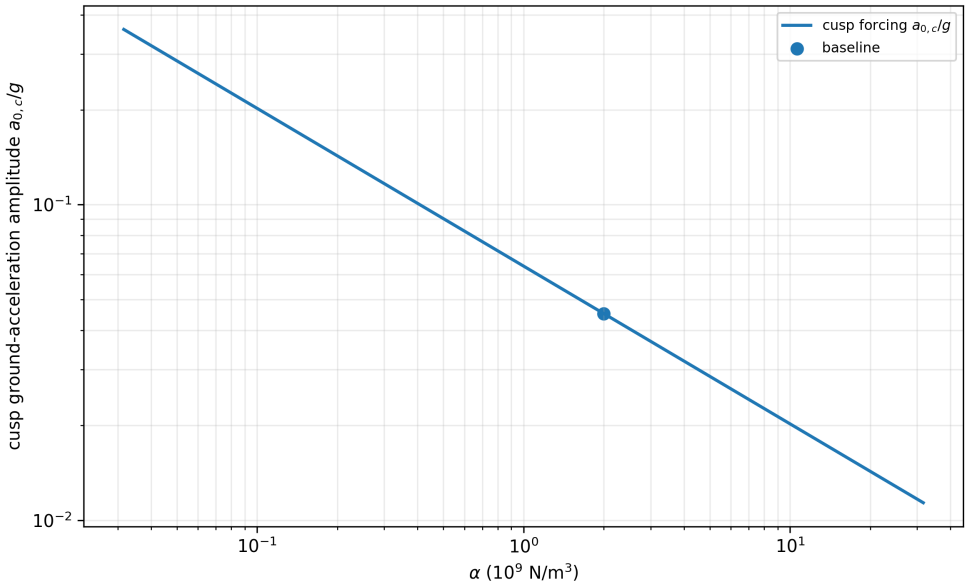


Figure 11: Cusp forcing versus positive cubic stiffness. The log–log slope follows the $|\alpha|^{-1/2}$ scaling, so the onset of multistability moves to arbitrarily large forcing in the linear limit.

Theorem 2 (Linear recovery and cusp escape)**.** *For nonzero damping and fixed finite forcing, the finite-amplitude harmonic branch of the linear–Duffing building converges to the unique linear response as $\alpha \to 0$. Simultaneously, the Duffing cusp requires forcing and response amplitude proportional to $|\alpha|^{-1/2}$; hence branch multiplicity is absent from the finite-response linear limit.*

10 Nonlinear-stiffness tuning for passive pounding mitigation

The preceding results show that nonlinearity can help or hurt. The natural next question is quantitative: *how should α be chosen, within the reduced model, to avoid a given gap from closing?* A convenient answer follows by parameterizing the Duffing harmonic state through its effective

dynamic stiffness

$$\Xi = \Delta_2 + \frac{3}{4}\alpha A_2^2. \tag{37}$$

The complex first-harmonic responses are

$$Z_1 = \frac{F_1}{\Delta_1 + id_1}, \qquad Z_2 = \frac{F_2}{\Xi + id_2}, \tag{38}$$

with $g_{\mathrm{cr}} = |Z_1 - Z_2|$. Because $A_2^2 = F_2^2/(\Xi^2 + d_2^2)$, the cubic coefficient associated with a selected Ξ is

$$\boxed{\alpha(\Xi) = \frac{4(\Xi - \Delta_2)(\Xi^2 + d_2^2)}{3F_2^2}}. \tag{39}$$

This relation is exact within first-harmonic balance and turns the nonlinear-stiffness selection problem into one-dimensional geometry in the complex-response plane.

Let $Z_1 = u + iv$. The boundary between safe and pounding harmonic states is $|Z_1 - Z_2| = g$. After substitution of Eq. (38), the boundary becomes the quadratic

$$(g^2 - |Z_1|^2)\Xi^2 + 2F_2 u\Xi + (g^2 - |Z_1|^2)d_2^2 - F_2^2 - 2F_2 v d_2 = 0. \tag{40}$$

Its real roots Ξ_- and Ξ_+ delimit the effective-stiffness values for which the phasor Z_2 lies inside the safe circle of radius g centered at Z_1, as shown in Figure 12.

The minimum of $|Z_1 - Z_2|$ with respect to Ξ can also be obtained analytically. Differentiation gives

$$u\Xi^2 - (F_2 + 2vd_2)\Xi - ud_2^2 = 0. \tag{41}$$

A physically admissible root Ξ_{opt} inserted into Eq. (39) gives α_{opt}.

For the representative case $\Omega/\omega_2 = 1.20$, $a_0 = 0.12g$ and $g = 0.10$ m, Eq. (40) gives

$$\Xi_- = 4.253 \times 10^6 \text{ N/m}, \qquad \Xi_+ = 3.590 \times 10^7 \text{ N/m}. \tag{42}$$

The corresponding nominal cubic-coefficient crossings are 1.131×10^9 and 1.837×10^{10} N/m^3. However, a nominally safe high-amplitude branch is not sufficient when another attracting branch can coexist. At the same forcing frequency the cubic discriminant changes sign at

$$\alpha_{D,-} = 0.883 \times 10^9, \qquad \alpha_{D,+} = 2.111 \times 10^9 \text{ N/m}^3. \tag{43}$$

Thus a conservative root-robust first-harmonic condition for the 0.10 m gap is

$$\boxed{2.111 \times 10^9 < \alpha < 1.837 \times 10^{10} \text{ N/m}^3}. \tag{44}$$

Within this interval the selected excitation admits no competing harmonic root with a gap demand

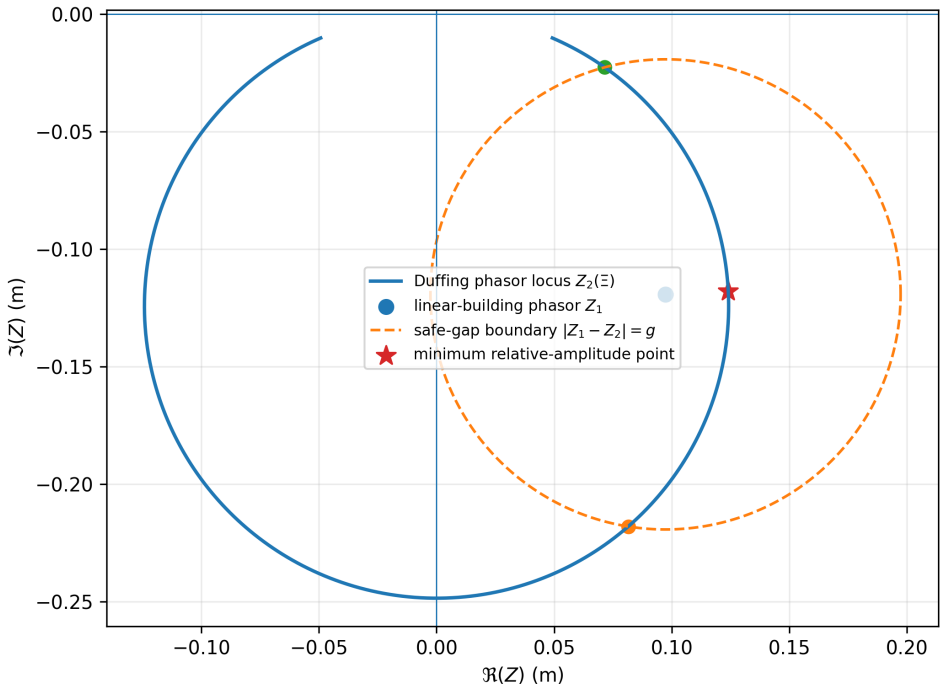


Figure 12: Phasor interpretation of nonlinear anti-pounding tuning at $\Omega/\omega_2 = 1.20$, $a_0 = 0.12g$ and $g = 0.10$ m. The nonlinear-building response $Z_2(\Xi)$ is safe whenever it lies inside the circle of radius g centered at the linear-building response Z_1. The star is the minimum-relative-response point.

above 0.10 m. The optimum from Eq. (41) is

$$\alpha_{\mathrm{opt}} = 2.442 \times 10^9 \ \mathrm{N/m^3}, \qquad g_{\mathrm{cr,min}}^{\mathrm{HB}} = 0.0267 \ \mathrm{m}. \tag{45}$$

Figure 13 shows the complete branch and root-robust dependence on α. The numerical tuning thresholds and optimum for this representative design case are summarized in Table 2.

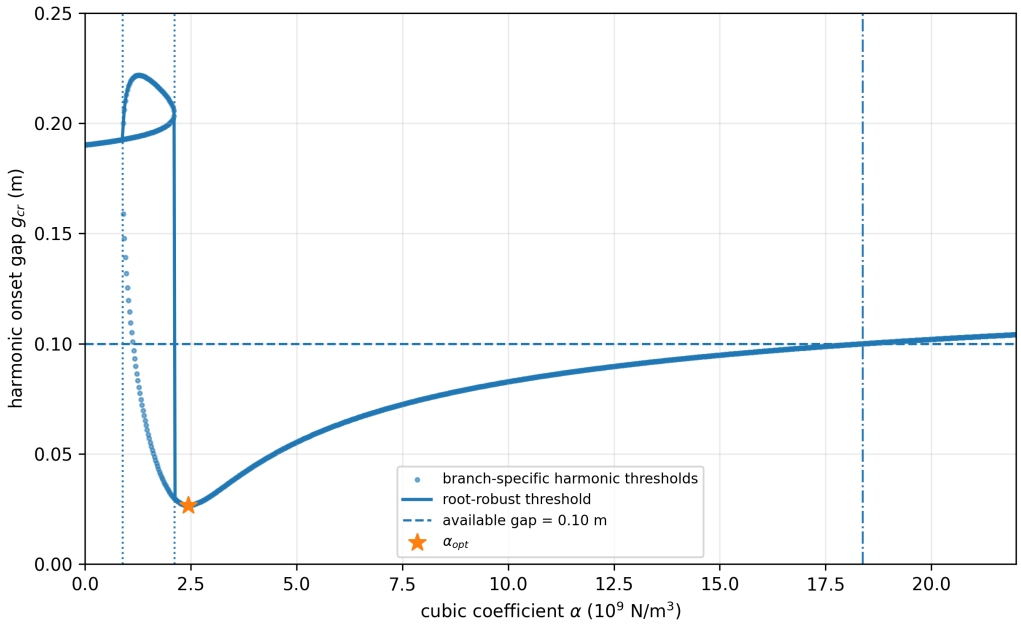


Figure 13: Harmonic onset gap versus cubic stiffness at $\Omega/\omega_2 = 1.20$ and $a_0 = 0.12g$. Dotted vertical lines are the two discriminant crossings; the dash-dotted line is the upper safe-gap crossing. The root-robust safe region for a 0.10 m gap begins immediately above the upper discriminant crossing and ends at the upper gap crossing.

Table 2: Nonlinearity-tuning results for the representative harmonic design point. Values are first-harmonic reduced-model predictions, not code-prescribed design limits.

Quantity	Value
Frequency ratio Ω/ω_2	1.20
Ground-acceleration amplitude	$0.12g$
Available clear gap	0.10 m
Discriminant crossings in α	0.883 and 2.111×10^9 N/m^3
Nominal safe-branch crossings	1.131 and 18.374×10^9 N/m^3
Root-robust safe interval	$2.111 < \alpha/(10^9) < 18.374$
Optimal coefficient α_{opt}	2.442×10^9 N/m^3
Minimum harmonic onset gap	26.7 mm

The interval in Eq. (44) is scenario-specific; it must be recomputed when the frequency content, intensity, damping, structural properties or available gap change. Its importance is conceptual: the

cubic coefficient can be treated as a passive anti-pounding tuning variable rather than only as an uncertainty. In practice this tuning could be pursued through nonlinear braces, elastic restraints, isolation hardware or other devices whose restoring curves are intentionally shaped. A design should also remain away from fold boundaries, because nominal gap reduction near a fold can be fragile to small changes in excitation or model parameters.

11 Engineering implications and limitations

11.1 What the nonlinear coefficient means

The coefficient α is an effective modal parameter, not a universal material constant. The inverted-pendulum calculation gives one geometric mechanism that produces $\alpha > 0$, while a reduced frame, brace or isolation model may produce either sign. For conventional reinforced-concrete or steel frames undergoing large inelastic excursions, a smooth cubic law cannot reproduce pinching, stiffness degradation, strength deterioration or residual drift. In such cases a Bouc–Wen, bilinear, fiber or other hysteretic model is more appropriate. The value of the Duffing model is that it isolates amplitude-dependent detuning and phase reorganization in analytically transparent form.

11.2 Why nonlinearity may be protective

The critical quantity is the relative response $x_1 - x_2$, not either building displacement individually. Consequently a larger nonlinear amplitude need not imply more danger. If the nonlinear stiffness moves the two responses toward phase synchronization, then g_{cr} can decrease even as A_2 increases. Conversely, a frequency shift toward an adverse phase relation can enlarge the relative demand. The new design equations make this distinction explicit: protection corresponds to moving Z_2 into the safe circle around Z_1 rather than simply minimizing $|Z_2|$.

11.3 Scope of the tuning result

Equation (44) is not a recommendation to assign a single universal cubic stiffness to a building. It is a reduced-order demonstration that there can exist a finite interval of nonlinear stiffness for which a specified joint remains open under a specified harmonic design scenario. The lower edge of that interval is controlled by branch multiplicity in the representative example, while the upper edge is controlled by loss of phasor synchronization. Both edges move with excitation frequency and intensity. For broadband earthquakes, the exact onset theorem remains valid, but the tuning problem should be formulated over a record set or a spectral uncertainty region rather than a single harmonic.

11.4 Limitations

The present model intentionally isolates one nonlinear mechanism in the smallest system that retains folds, jumps, phase switching and unilateral contact. It does not include higher structural modes,

floor-to-floor impact, torsion, bidirectional motion, soil–structure interaction, nonproportional damping, strength degradation, residual drift, stochastic gap uncertainty or pounding-induced local damage. The Hertz parameters are illustrative and peak forces should not be transferred directly to a real joint without contact calibration. First-harmonic balance is used only for pre-impact periodic states; it loses accuracy when higher harmonics are large. By contrast, the exact onset criterion remains valid if the pre-impact trajectories are generated by a more sophisticated MDOF or finite-element model.

The practical role of the present theory is therefore screening and mechanism identification. It can identify combinations of frequency, intensity, nonlinear stiffness and gap for which detailed analysis is most necessary, and it can indicate whether a nonlinear device is likely to move the structure toward or away from a favorable relative-response phase.

12 Conclusions

This study examined seismic pounding between adjacent structures when one building exhibits amplitude-dependent lateral stiffness before contact. The resulting problem differs from the conventional linear–linear case because nonlinear detuning changes both response amplitude and phase, and therefore changes the relative displacement that governs closure of the seismic joint.

The main engineering findings are:

1. For arbitrary common ground acceleration, the exact first-impact threshold is the maximum pre-contact oriented relative displacement, $g_{\mathrm{cr}} = \max_t[x_1^{(0)} - x_2^{(0)}]$. The threshold is independent of the post-contact stiffness and damping parameters.

2. Under harmonic excitation, the Duffing response reduces to a cubic equation in the squared amplitude. Its transition boundaries identify where multiple pre-impact response states can coexist and therefore where the required seismic separation becomes branch dependent.

3. At $\Omega/\omega_2 = 1.20$ and $a_0 = 0.12g$, the representative lower nonlinear state requires approximately 0.200 m of clearance, while a coexisting higher-amplitude state requires only about 0.034 m because the structures move nearly in phase. Joint demand therefore cannot be inferred reliably from individual peak displacements alone.

4. Direct Hertz-type simulations reproduce the predicted transition between pounding and impact-free response. For the representative 0.10 m gap, the adverse response basin produces repeated impacts whereas the favorable coexisting basin remains contact-free.

5. Treating the effective cubic stiffness as a design variable yields a scenario-specific root-robust safe interval $2.111 \times 10^9 < \alpha < 1.837 \times 10^{10}$ N/m^3. The reduced model gives an optimum near 2.442×10^9 N/m^3, for which the harmonic onset gap is about 26.7 mm.

6. Broadband excitation confirms that the general onset theorem is not restricted to steady harmonic motion. Harmonic-response boundaries are best interpreted as a mechanism-exposing design tool embedded within the more general pre-impact criterion.

The principal design implication is that appropriately shaped structural nonlinearity can be protective as well as adverse. Passive mitigation should therefore target the relative amplitude and phase across the seismic joint rather than the displacement of either building in isolation. The proposed onset criterion and separation-gap maps are intended as an inexpensive screening layer before detailed multi-degree-of-freedom, finite-element and calibrated contact analyses. Their use does not replace code-prescribed separation requirements; instead, they identify parameter regions and excitation scenarios in which nonlinear interaction merits more detailed assessment.

13 Future work

Several extensions follow naturally from the present results. First, the scalar Duffing mode should be embedded in multi-storey shear-frame and finite-element models so that the reduced coefficient α can be identified from pushover curves, nonlinear modal reduction or component-level constitutive laws. Second, the anti-pounding tuning problem should be reformulated for suites of recorded ground motions, with α selected to minimize a robust statistic of $\max_t(x_1 - x_2)$ rather than a single harmonic quantity. Third, hysteretic models such as Bouc–Wen, bilinear and degrading restoring laws should be examined to determine which parts of the discriminant/phasor picture survive when the response is history dependent and non-smooth.

Further work should also include torsion and bidirectional excitation, unequal floor elevations, soil–structure interaction, uncertainty in joint width and impact stiffness, and local damage criteria. From a design perspective, a particularly interesting direction is to realize tunable nonlinear stiffness through braces, inerter-based devices, nonlinear elastic restraints or semi-active elements, and then optimize the device so that the relative-response phasor remains inside a prescribed safe region over a frequency–intensity uncertainty set. Finally, experimental validation on a two-structure shake-table configuration would provide a direct test of the predicted transition from harmful to protective nonlinearity and of the abrupt changes in pounding demand near nonlinear branch jumps.

Data and code availability

The numerical parameters and plotted results required to interpret the study are reported in the manuscript and supplied figures. The source manuscript and high-resolution figure files accompany the submission. Additional computational scripts and intermediate numerical data are available from the corresponding author upon reasonable request.

Funding

No external funding was received for this study.

Declaration of competing interest

The authors declare no competing interests.

Author contributions

Both authors contributed to the development and interpretation of the study, reviewed the manuscript, and approved the submitted version. The corresponding author coordinated the analytical and computational preparation of the manuscript.

AI disclosure

Generative artificial intelligence was used as an authoring aid for language refinement, mathematical typesetting support and code drafting under human supervision. The authors retain responsibility for the derivations, numerical verification, interpretation, references and final manuscript content.

References

[1] Anagnostopoulos SA. Pounding of buildings in series during earthquakes. *Earthquake Engineering & Structural Dynamics*. 1988;16(3):443–456. doi:10.1002/eqe.4290160311.

[2] Papadrakakis M, Mouzakis H, Plevris N, Bitzarakis S. A Lagrange multiplier solution method for pounding of buildings during earthquakes. *Earthquake Engineering & Structural Dynamics*. 1991;20(11):981–998. doi:10.1002/eqe.4290201102.

[3] Maison BF, Kasai K. Dynamics of pounding when two buildings collide. *Earthquake Engineering & Structural Dynamics*. 1992;21(9):771–786. doi:10.1002/eqe.4290210903.

[4] Anagnostopoulos SA, Spiliopoulos KV. An investigation of earthquake induced pounding between adjacent buildings. *Earthquake Engineering & Structural Dynamics*. 1992;21(4):289–302. doi:10.1002/eqe.4290210402.

[5] Jeng V, Kasai K, Maison BF. A spectral difference method to estimate building separations to avoid pounding. *Earthquake Spectra*. 1992;8(2):201–223. doi:10.1193/1.1585679.

[6] Kasai K, Maison BF. Building pounding damage during the 1989 Loma Prieta earthquake. *Engineering Structures*. 1997;19(3):195–207. doi:10.1016/S0141-0296(96)00082-X.

[7] Jankowski R. Non-linear viscoelastic modelling of earthquake-induced structural pounding. *Earthquake Engineering & Structural Dynamics*. 2005;34(6):595–611. doi:10.1002/eqe.434.

[8] Muthukumar S, DesRoches R. A Hertz contact model with non-linear damping for pounding simulation. *Earthquake Engineering & Structural Dynamics*. 2006;35(7):811–828. doi:10.1002/eqe.557.

[9] Jankowski R. Earthquake-induced pounding between equal height buildings with substantially different dynamic properties. *Engineering Structures*. 2008;30(10):2818–2829. doi:10.1016/j.engstruct.2008.03.006.

[10] Ye K, Li L, Zhu H. A note on the Hertz contact model with nonlinear damping for pounding simulation. *Earthquake Engineering & Structural Dynamics*. 2009;38(9):1135–1142. doi:10.1002/eqe.883.

[11] Fiore A, Marano GC, Monaco P. Earthquake-induced lateral-torsional pounding between two equal height multi-storey buildings under multiple bi-directional ground motions. *Advances in Structural Engineering*. 2013;16(5):845–865. doi:10.1260/1369-4332.16.5.845.

[12] Miari M, Choong KK, Jankowski R. Seismic pounding between adjacent buildings: Identification of parameters, soil interaction issues and mitigation measures. *Soil Dynamics and Earthquake Engineering*. 2019;121:135–150. doi:10.1016/j.soildyn.2019.02.024.

[13] Elgammal A, Seleemah A, Elsharkawy M, Elwardany H. Comprehensive review on seismic pounding between adjacent buildings and available mitigation measures. *Archives of Computational Methods in Engineering*. 2024;31:4269–4304. doi:10.1007/s11831-024-10114-6.

[14] Nayfeh AH, Mook DT. *Nonlinear Oscillations*. New York: Wiley; 1979.

[15] Kovacic I, Brennan MJ, editors. *The Duffing Equation: Nonlinear Oscillators and their Behaviour*. Wiley; 2011.

[16] Chopra AK. *Dynamics of Structures: Theory and Applications to Earthquake Engineering*. 5th ed. Pearson; 2017.

[17] American Society of Civil Engineers. *ASCE/SEI 7-22: Minimum Design Loads and Associated Criteria for Buildings and Other Structures*. Reston, VA: ASCE; 2022.

[18] CEN. *EN 1998-1: Eurocode 8: Design of Structures for Earthquake Resistance – Part 1*. Brussels: European Committee for Standardization; 2004.

Supplementary Files

This is a list of supplementary files associated with this preprint. Click to download.

- BulletinofEarthquakeEngineeringVUGAR.zip